Jansen, V.A.A. (1994). On the bifurcation structure of two diffusively coupled predator-prey systems. In: Jansen, V.A.A. (1994), Theoretical Aspects of Metapopulation Dynamics, PhD thesis, University of Leiden, the Netherlands

7

On the bifurcation structure of two diffusively coupled predator-prey systems

Summary

A model for a predator and prey population, living in two patches is analysed. Within a patch the prey grows logistically and the predators react to local prey densities with a Holling type II functional response. The two patches are coupled through predator migration. The system is a model for a simple predator-prey metapopulation in which the local densities are described explicitly, but also is a caricature of a spatially distributed predator-prey system. The dynamical behaviour of the system is described using one and two parameter bifurcation diagrams. Two types of attractors are identified in which lasting differences between the densities in the patches exist. For small predator migration rates attractors exist where the local (i.e. within patch) dynamics are asynchronous. The attractors can be periodic, quasi-periodic or chaotic. For large predator migration rates attractors in the form of equilibria or limit cycles exist, in which one of the patches contains no prey. The relation between these different attractors is described using one and two parameter bifurcation diagrams. The results show that asynchronous local dynamics arise spontaneously in metapopulations and that the fluctuations of a metapopulation can be reduced compared to the fluctuations of a single isolated population. Moreover, they show that spatial predator-prey populations can be regulated through the interplay of local dynamics and migration. For this regulation no density dependence at the level of the individual is needed so that enrichment of the environment does not necessarily have the paradoxical consequence that prey and predator densities reach levels where extinction is likely to occur.

7.1 Introduction

Regulation of population densities is mostly effected in mathematical models through a negative feedback of the population densities on the *per capita* vital rates. Mathematical models of predator-prey systems with density dependence at the level of the individual often predict extreme fluctuations in densities, such that the predator and prey populations repeatedly reach very low densities (Rosenzweig, 1971 and 1972). In many data series of predator-prey systems fluctuations can be observed, but these are normally not as vigorous as the fluctuations predicted by mathematical models. The difference between the observed dynamical behaviour of natural populations and that predicted by such mathematical models suggests that natural predator-prey populations are not exclusively regulated by density dependence at an individual level.

An example of a regulatory mechanism that does not directly operate at individual level is provided by so called "metapopulation" models. A metapopulation consists of a set of local populations that are coupled through migrations. (For a review on metapopulation theory see Gilpin & Hanski (1991) and Hastings & Harrison, (in prep.)). A metapopulation persists when local populations go through cycles of colonization and subsequent extinction, as long as these cycles proceed asynchronously (Taylor, 1990). In a predator-prey metapopulation it is not difficult to imagine that the local populations can go through large fluctuations, perhaps actually going extinct, but that at the metapopulation level these cycles are damped when the local oscillations proceed out of phase. The regulation then is not only at the level of the individual but also at (local) population level.

In itself this may sound as a truism: when local dynamics proceed out of phase the effects of local fluctuations will simply average out in the regional densities. However, this argument hinges on the asynchrony of the fluctuations in the local densities. The crucial question thus is whether or not asynchronous fluctuations in the local densities are to be expected in metapopulations. One of the requirements of a metapopulation is migration between local populations (Hanski, 1991). Migration tends to reduce differences. When no differences between the local populations exist, the local densities fluctuate in phase. If phase differences between the fluctuations in the local densities really are an intrinsic property of metapopulations, metapopulations must then counteract the equalizing force of diffusion.

There is some empirical evidence that asynchronous local dynamics occurs in actual metapopulations (Nachman, 1991; Van de Klashorst *et al.*, 1992). Asynchronous local dynamics has also been demonstrated in simulation studies (Hassell *et al.*, 1991; Comins *et al.*, 1992), in two patch host parasitoid models (Adler, 1993) and in simple analytic models for a single species metapopulation (Gyllenberg *et al.*, 1993; Hastings, 1993). Despite this there is no complete understanding how and when asynchronous local dynamics may appear.

In this paper we demonstrate the existence of lasting differences in local

densities in predator-prey models and the conditions under which these arise naturally from the interplay of the local population dynamics and the spatial interactions between local populations. The metapopulation we use here is the simplest thinkable: a system of two identical patches whose dynamics are coupled through migration of individuals. The work in this paper builds on results presented in a previous paper where we studied two diffusively coupled identical patches (Jansen, in prep.), the dynamics in each patch being defined by the Lotka-Volterra equations. For this system it was shown that, although eventually all spatial differences vanish, closed orbits on which the local densities oscillate in phase with a large amplitude are unstable for appropriate choices of parameters and that orbits starting from nearby initial conditions converge towards closed orbits with in phase local oscillations with a small amplitude. Here we will proceed similarly and show that in a two patch metapopulation, where the local dynamics corresponds to a predator-prey system with logistic prey growth and a Holling type II functional response, limit cycles with in phase oscillations can be unstable for small predator migration rates. The limit cycles that branch off the limit cycle with in phase oscillations connect, when parameters are varied, to stable attractors with out of phase oscillations. Furthermore we will show that for large predator migration rates stable equilibria or limit cycles, in which the local predator and prey densities differ, exist. As an appetizer, Figure 7.1 shows some of the different types of dynamics for our predator-prey system. We finally address the case where the prey growth is exponential instead of logistic and show that also in this case stable attractors with out of phase oscillations exist.

The model studied here deserves attention not only for its biological significance but also for its surprisingly rich dynamical behaviour. We have found periodic, quasi-periodic and chaotic attractors in all of which the local dynamics proceed out of phase. By means of one and two parameter bifurcation diagrams we will describe the "genesis" of these attractors. When prey growth is exponential instead of logistic we have partly revealed the bifurcation structure.

Our results show that through the interplay of local dynamics and migration asynchronous oscillations can arise and that the fluctuations in the total densities are damped compared to the fluctuations in a single isolated population. Our results have a wider significance, however. The one but crudest discretisation of space is a subdivision in two regions. The model used here can serve as a caricature of predator-prey systems in a spatially homogeneous environment. This leads us to the conclusion that spatial interactions can regulate predator-prey populations, even in absence of regulatory mechanism at the level of the individual .

7.2 Model description

We describe the local interaction between predator and prey by a special case of the Rosenzweig-Mac Arthur (1963) model in which the prey population is

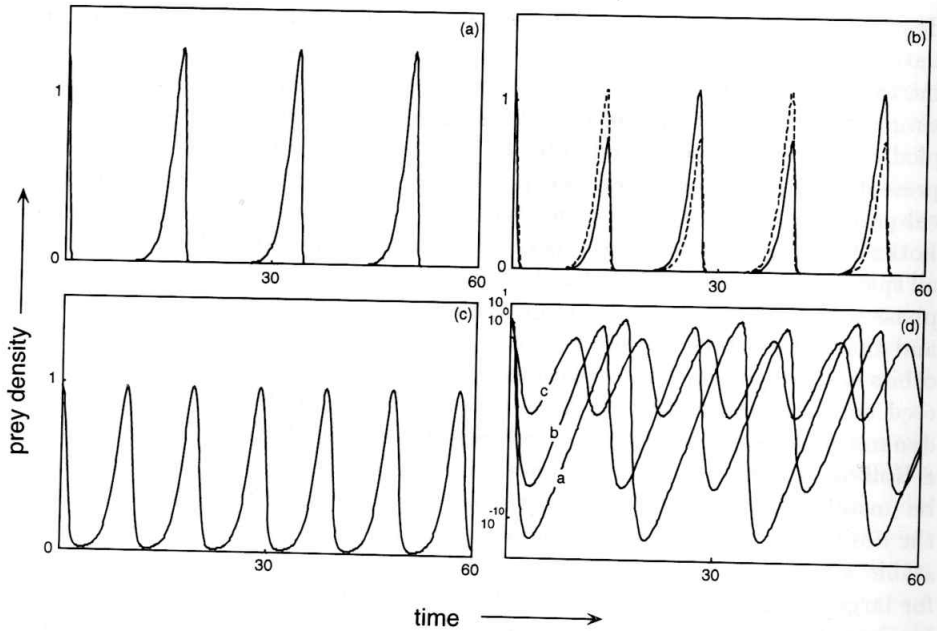

Figure 7.1: The prey density versus time for some attractors of system (7.2) with the parameters $r = \mu = 1$, $b = 9.96$, $c = 2b$, $d_n = 0$. The prey density in patch 1 is represented by a drawn line, the prey density in patch 2 by a dashed line. (a) A stable limit cycle in which the densities in the patches are equal, the dashed line is therefore not visible. The limit cycle is stable for $d < 0.275$ and $d > 0.558$. The fluctuations are identical to those in a predator-prey system in a single, isolated patch. (b) A stable limit cycle for $d = 0.675$ in which the densities in the patches fluctuate out of phase with a phase difference of half a period. (c) A stable limit cycle for $d = 20$ in which the prey density in patch 2 is zero. The predator densities fluctuate in both patches. (d) the logarithm of the average prey densities for the limit cycles in (a), (b) and (c).

growing logistically and the predator has a Holling type II functional response:

$$\begin{aligned} \frac{dN}{dt} &= rN(1-\tfrac{N}{c}) \quad -\tfrac{NP}{1+N/b} \\ \frac{dP}{dt} &= \tfrac{NP}{1+N/b} \quad -\mu P \end{aligned} \tag{7.1}$$

The variable N denotes the density of the prey population and P the density of the predator population. The parameters have the following interpretation:

r: prey growth rate at low prey densities,
c: carrying capacity of the prey population,
b: the saturation value of the functional response,
μ: the predator death rate in absence of prey.

The variables in (7.1) are already scaled to reduce the number of parameters. The scaling chosen preserves the carrying capacity, which is the factor that predominantly expresses regulation, as a bifurcation parameter. Furthermore, by taking the limit of c and b tending to infinity, system (7.1) reduces to the Lotka-Volterra system.

Now a two patch metapopulation with identical patches in which the local dynamics are defined by (7.1) is described by:

$$\begin{array}{rcccl} \frac{dN_i}{dt} & = & rN_i(1-\frac{N_i}{c}) & -\frac{N_iP_i}{1+N_i/b} & +d_n(N_j-N_i) \\ \frac{dP_i}{dt} & = & \frac{N_iP_i}{1+N_i/b} & -\mu P_i & +d(P_j-P_i) \end{array} \qquad i,j \in \{1,2\}; \quad i \neq j \tag{7.2}$$

where N_i and P_i denote the densities of the prey and predator population in patch i. The parameters d_n and d denote the *per capita* migration rate of, respectively, prey and predator.

We note that, since the parameters describing the within patch dynamics are identical for both patches, system (7.2) is symmetrical. By defining the reflection operator R, as:

$$R(x,y,u,v) = (u,v,x,y)$$

it can be seen immediately that when $S(t) = (N_1(t), P_1(t), N_2(t), P_2(t))$ is a solution of (7.2), $RS(t)$ is also a solution. Moreover, the diagonal subspace $D = \{(N_1, P_1, N_2, P_2) \in \mathbb{R}^4_+ | N_1 = N_2, P_1 = P_2\}$ is symmetrical in the sense that $RD = D$. It can be seen directly from the equations that when the densities in both patches are equal, migration has no effect and hence D is invariant. On D the dynamics of N_i and P_i are given by (7.1). The dynamics of (7.1) are well known. System (7.1) allows for a single two species equilibrium. This equilibrium can be either locally stable or unstable. If the equilibrium is unstable a stable limit cycle exists. Hence, when the parameters are chosen such that for (7.1) a stable limit cycle exists, system (7.2) also has a symmetrical limit cycle $\Gamma(t)$ with $R\Gamma(t) = \Gamma(t)$ in which at every moment in time the densities in the two patches are equal and so the fluctuations in the local densities are strictly in phase. In order to locate asymmetric attractors of (7.2), we will study the stability of the equilibria and of the symmetric limit cycle Γ and continue the solutions that bifurcate off these solutions. Guided by the observations on two coupled patches with Lotka-Volterra local dynamics (Jansen, submitted *b*) the other parameters were fixed at: $r = \mu = 1, b = 9.96, d_n = 0$. For the parameter values chosen all equilibria of (7.1) are unstable and the two species equilibrium is surrounded by a stable limit cycle. As bifurcation parameter we have used d, which expresses the coupling between the two patches. As a second bifurcation parameter we have used c, which represents the carrying capacity. For location and continuation of equilibria and limit cycles the program "LOCBIF" (Khibnik *et al.*, 1993) has been used.

E_{00}	$(0,0,0,0)$
E_{01}	$(0,0,c,0)$
E_{11}	$(c,0,c,0)$
E_{12}	$\left(0, \frac{dr}{\mu^2+2d\mu}\tilde{N}(1-\frac{\tilde{N}}{c}), \tilde{N}, \frac{r(\mu+d)}{\mu^2+2d\mu}\tilde{N}(1-\frac{\tilde{N}}{c})\right)$
E_{22a}	$\left(N^*, \frac{r}{\mu}N^*(1-\frac{N^*}{c}), N^*, \frac{r}{\mu}N^*(1-\frac{N^*}{c})\right)$
E_{22b}	$\left(\hat{N}_a, r(1-\frac{\hat{N}_a}{c})(1+\frac{\hat{N}_a}{b}), \hat{N}_b, r(1-\frac{\hat{N}_b}{c})(1+\frac{\hat{N}_b}{b})\right)$
$\tilde{N}$	$(\frac{\mu+d}{\mu^2+2d\mu}-\frac{1}{b})^{-1}$
N^*	$(\frac{1}{\mu}-\frac{1}{b})^{-1}$
$\hat{N}_a$	$\frac{1}{2}(c-N^*)-\gamma+\frac{1}{2}\sqrt{(c-3N^*-2\gamma)(N^*+c+2\gamma)}$
$\hat{N}_b$	$\frac{1}{2}(c-N^*)-\gamma-\frac{1}{2}\sqrt{(c-3N^*-2\gamma)(N^*+c+2\gamma)}$
γ	$\frac{b(2d\mu+\mu^2-bd-b\mu))}{(b-\mu)(b-\mu-2d)}$

Table 7.1: Equilibria of (7.2) with $d_n = 0$. Three more equilibria are possible which are R images of the equilibria not lying in D: $E_{01} = RE_{01}$, $E_{21} = RE_{12}$ and $E_{22c} = RE_{22b}$.

7.3 Bifurcation structure

The bifurcation diagram of (7.2) is rather complex. We therefore start with describing the equilibria and the behaviour for $d = 0$, followed by the bifurcation structure within the face $N_2 = 0$, i.e. when no prey is present in patch 2. Within this invariant subspace less ω-limit sets exist than in the complete state space. In two separate subsections we will describe the connections between ω-limit sets in $\mathbb{R}^4_+$ and those in the faces $N_i = 0$.

7.3.1 Equilibria

System (7.2) with d_n equal to zero maximally allows for nine equilibria (see Appendix). These equilibria are listed in Table 7.1. The equilibria are denoted by E_{ij} where i refers to the number of species in patch 1 and j to the number of species in patch 2. When more equilibria are possible for a certain combination a letter added to the subscript indicates this.

The equilibria E_{00}, E_{11} and E_{22a} all lie in D and correspond to the equilibria of (7.1) with identical equilibrium densities in both patches. Equilibrium E_{00} is always a saddle, E_{11} is stable for $c < 1$ and a saddle otherwise. Equilibrium E_{22a} is positive iff $c > \frac{b\mu}{b-\mu}$ and stable as long as $c \leq b\frac{b+\mu}{b-\mu}$. When increasing c, E_{22a}, is subject to a Hopf bifurcation and is subsequently surrounded by the symmetrical limit cycle Γ. The equilibrium E_{22a} can not lose its stability otherwise than in a Hopf bifurcation (Segel & Jackson, 1972). When E_{22a} is unstable it can undergo a pitchfork bifurcation in which E_{22b} and E_{22c} branch off.

Since we restricted ourselves to the case $d_n = 0$, four equilibria are possible in which one of the patches contains no prey. These equilibria lie within one of the invariant subspaces $\{(N_1, P_1, N_2, P_2) \in \mathbb{R}^4_+ | N_i = 0, i = 1, 2\}$ to which we will

further refer as the faces $N_i = 0$. The equilibria in which the densities are not identical always have a symmetrical counterpart so that in total nine equilibria are possible The computation of the equilibria is given in the Appendix.

7.3.2 Decoupled patches

When both migration rates are equal to zero the two patches are decoupled and the dynamics in both patches are described by (7.1). For the parameters chosen, system (7.1) allows a stable limit cycle and three unstable equilibria with zero, one or two species present. In the decoupled system therefore nine equilibria exist which consist of combinations of equilibria of (7.1), six limit cycles exist which consist of a combination of an equilibrium of (7.1) in one patch and the limit cycle of (7.1) in the other patch and an invariant torus exists, when both patches are on the limit cycle of (7.1).

The nine equilibria are listed in Table 7.1. In the equilibrium E_{00} both patches are empty and in E_{10} and E_{01} one patch is at the one species equilibrium while the other patch is empty. In E_{11} we have the one species equilibrium in both patches where in E_{22a} both patches are at the two species equilibrium. As can be seen from Table 7.1 the equilibria E_{12} and E_{12} for $d = 0$ correspond to the case where one patch is empty and the other is at the two species equilibrium. Finally E_{22b} and E_{22c} for $d = 0$ represent the cases where one patch is at the one species equilibrium while the other is at the two species equilibrium. Since all equilibria of (7.1) are unstable for the choice of parameters used here, all equilibria of (7.2) are unstable for small d. Furthermore we note that for small positive d the equilibria E_{22b} and E_{22c} have a negative predator density in one of the patches.

Six other ω-limit sets exist for $d = 0$ consist of combinations of a limit cycle in one patch and an equilibrium in the other patch. Since (7.1) allows for three equilibria, three different combinations can be formed and since every combination has an R image we come to six ω-limit sets. Since for the choice of parameters used here all equilibria of (7.1) are unstable, for small d no stable ω-limit sets formed out of a combination of equilibrium and limit cycle exist. Four of these limit cycles could be detected with the continuation procedure used and for small d all four are unstable. The two limit cycles at $d = 0$ corresponding to the combinations of the limit cycle and the one species equilibrium, could not be continued but simulation runs of (7.2) gave clear indication that they do not give rise to positive stable ω-limit sets.

For $d = 0$ also an invariant torus exists, corresponding to the state where both patches exhibit limit cycles (possibly with a phase difference). The invariant torus contains the symmetrical limit cycle Γ. The symmetrical limit cycle and a limit cycle in which the fluctuations in the patches have a phase difference of π are the only limit cycles stemming from the invariant torus that could be continued for small d. The symmetrical limit cycle is the only attractor for small d, all other ω-limit sets are unstable.

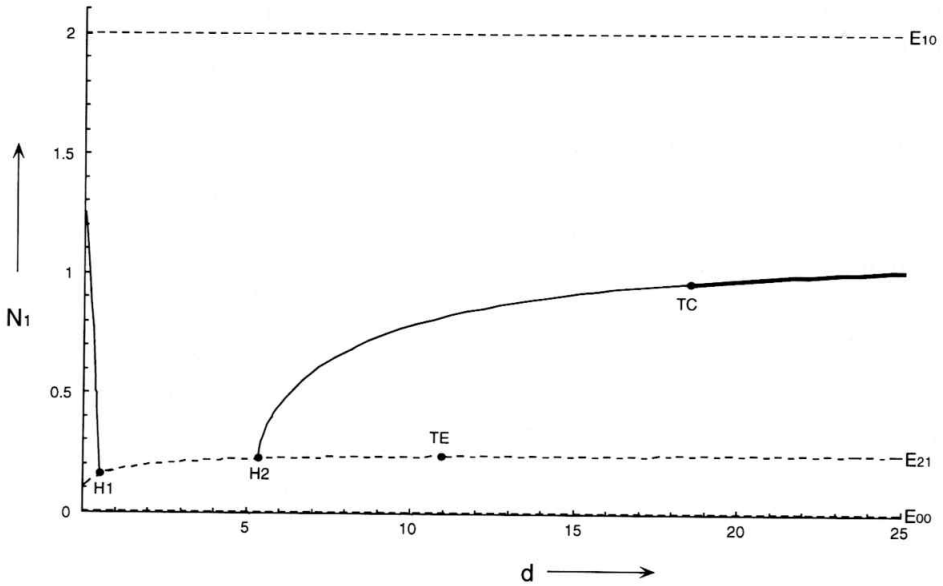

Figure 7.2: A one parameter bifurcation diagram in d for (7.2) in which only the branches in the face $N_2 = 0$ are drawn. On the vertical axis the value of N_1 in the equilibria and the maximum of N_1 for limit cycles is given. Dashed lines represent unstable equilibria, thin drawn lines unstable limit cycles and thick drawn lines stable limit cycles. Black dots indicate bifurcations. Labels: H1, H2: Hopf bifurcations, TC: transcritical bifurcation of limit cycles, TE: transcritical bifurcation of equilibria. Parameter values as in figure 7.1.

It is often stated that in metapopulations the migration rates should be not too small because then the metapopulation will behave like a system of decoupled local populations. This implies that some of the ω-limit sets that exist for zero migration rates will be stable for small migration rates. For system (7.2) such a statement does not hold: all ω-limit sets that exist for $d = 0$ are unstable for small d, the only exception being the symmetrical limit cycle. We will show that asymmetrical attractors do exist, but that they are not directly connected to the structures that exist for $d = 0$.

7.3.3 One patch without prey

Figure 7.2 gives the bifurcation structure within the face $N_2 = 0$, i.e., when no prey is present in patch 2. For $d = 0$ only three ω-limit sets with positive prey densities in patch 1 exist, being the prey-only equilibrium E_{10}, the predator-prey equilibrium E_{21} and a limit cycle formed out of the combination of a limit cycle in patch 1 while patch 2 is empty. All these ω-limit sets are unstable for small d.

Starting from $d = 0$ the ω-limit sets can be continued in d. The topmost

horizontal line denotes E_{10}; the equilibrium is always unstable and no bifurcations from it were found. The limit cycle corresponding to the situation at $d = 0$ where patch 2 is empty while the densities in patch 1 follow a limit cycle is always unstable but is a stable attractor within the face $N_2 = 0$. The limit cycle is unstable with respect to introduction of prey in patch 2. For increasing d this limit cyle shrinks and connects to equilibrium E_{21} in the Hopf bifurcation labelled in Figure 7.2 with H1 (in what follows we will simply refer to figure labels in the text by putting them between brackets). In Hopf bifurcation (H1) the stability of the limit cycle within the face $N_2 = 0$ is transferred to E_{21}. The equilibrium is unstable because it has an eigenvector transversal to the face $N_2 = 0$ with positive corresponding eigenvalue.

For larger d E_{21} goes through a second Hopf bifurcation (H2). The limit cycle that branches off attracts within the face $N_2 = 0$ but initially is unstable. When d is increased further first a transcritical bifurcation of equilibria (TE) can be detected on E_{21}. For still larger d the limit cycle that came into existence at (H2) goes through a transcritical bifurcation of cycles (TC) in which the limit cycle in the face $N_2 = 0$ gains stability. This limit cycle now is stable against introduction of small amounts of prey; when introduced in patch 2 they will go extinct because they will be consumed quickly by the predators in patch 2 which are feeded into this patch from patch 1. No other ω-limit sets with positive prey values in patch 1 were found.

7.3.4 Small predator migration rates

In this subsection we will give a detailed description of the bifurcation structure in $\mathbb{R}^4_+$ for small predator migration rates. Figure 7.3 summarizes this subsection. Later we will describe the series of events that leads to the stability of the limit cycle in Figure 7.2 for large predator migration rates. The ω-limit sets described in the previous subsection are also depicted in Figure 7.3. Figure 7.4a gives the phase portrait of the limit cycle that connects to E_{21} in Hopf bifurcation (H1). For small values of d the predator density in the equilibria E_{22b} and E_{22c} are negative in one of the patches and therefore not shown in the figure. In addition to the equilibria given in Figure 7.2 the equilibrium E_{22a} exists. For the choice of the other parameters used here, this equilibrium is always unstable within D, hence E_{22a} is unstable for all d. For increasing d a limit cycle approaches E_{22a} and connects to it in a Hopf bifurcation (H3). Due to the symmetry this limit cycle approaches the equilibrium from a direction transversal to D. As the phase portrait of this limit cycle (Fig. 7.4b) indicates, on the limit cycle the local oscillations have a phase difference of π. For $d = 0$ this limit cycle lies in the invariant torus described in the previous subsection.

Two limit cycles bifurcate off this limit cycle in a pitchfork bifurcation of limit cycles (PC). For increasing d these limit cycles disappear in a saddle-node bifurcations of limit cycles (F1a, F1b). In the saddle node bifurcation, to which we will further refer as a fold bifurcation, the limit cycles meet two other limit cy-

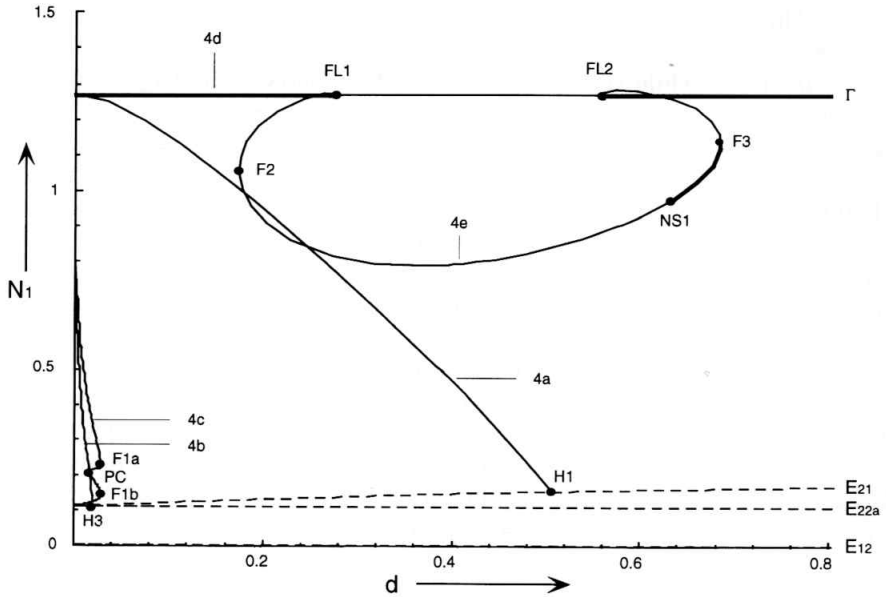

Figure 7.3: A one parameter bifurcation diagram for (7.2) for small values of d, giving the value of N_1 in the equilibria and the maximum of N_1 for limit cycles. The legends for lines and labels is given in figure 7.2; numbers refer to the phase portraits in figure 7.4. Additional labels: F1a, F1b, F2, F3: fold bifurcations of limit cycles, FL1, FL2 : flip bifurcations, H3: Hopf bifurcation, NS1: Neimark-Sacker bifurcation, PC: pitchfork bifurcation of limit cycles. Parameter values as in figure 7.1.

clesin which at $d = 0$ the densities in one patch are at the two species equilibrium, while they lie on limit cycle for the other (phase portrait given in Figure 7.4c). All these limit cycles are unstable.

We will next turn to the only stable ω-limit set that exists for small d: the symmetrical limit cycle Γ (phase portrait shown in Figure 7.4d). This limit cycle is stable for small d, then loses stability with increasing d in a flip bifurcation (FL1) and for still larger d gains stability, again in a flip bifurcation (FL2). Both flip bifurcations are subcritical: close to the bifurcations an unstable limit cycle with a period of approximately twice the period of Γ exists, while Γ is stable. The unstable limit cycles formed in the flip bifurcations disappear in fold bifurcations (F2, F3). The phase portrait of the limit cycle which is met in the fold bifurcation is given in Figure 7.4e. This limit cycle is stable close to (F3) and loses stability for decreasing d in a Neimark-Sacker bifurcation (NS1). In this bifurcation an invariant torus forms around the limit cycle and the stability is transferred to a quasi-periodic solution living on the invariant torus. (For this bifurcation the name Hopf bifurcation is also used. Since the bifurcation is not equivalent to a Hopf bifurcation from an equilibrium we use the name Neimark-Sacker bifurcation throughout this paper for the formation of an invariant torus

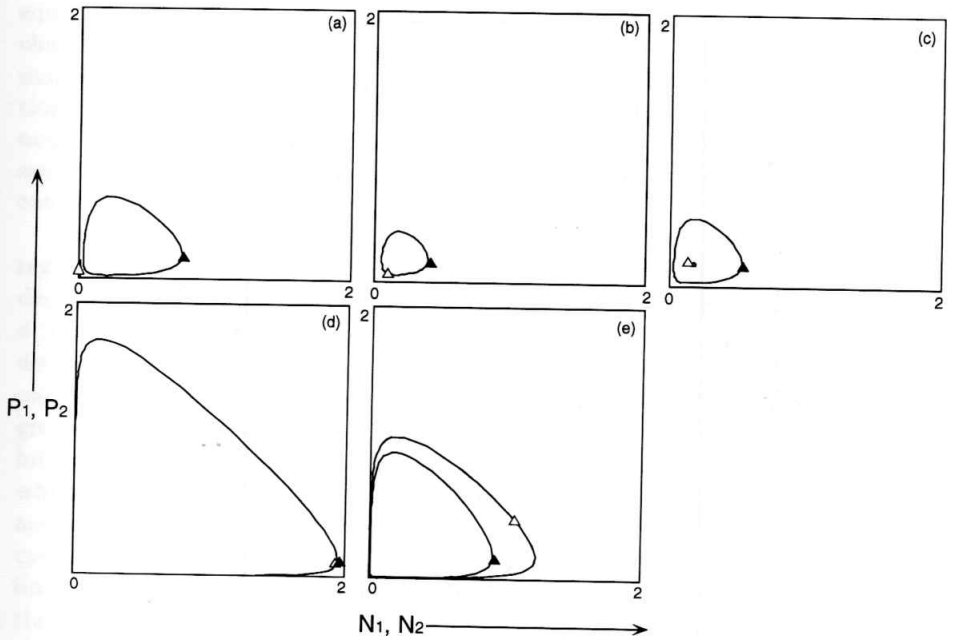

Figure 7.4: Phase portraits for a number of limit cycles in figure 7.3. The solid and open triangles give the position of the densities at the same moment for the densities in the two patches. For the symmetrical limit cycle in (d) the solid and open triangles superimpose.

around a limit cycle).

Figure 7.3 does not show an attractor in the d-region where Γ is unstable. The dynamical behaviour in this region can be clarified using a two parameter bifurcation diagram. In Figure 7.5 the fold bifurcations of cycles (F2, F3), the flip bifurcations (FL1, FL2) and the Neimark-Sacker bifurcation (NS1) are continued. We first note that the flip bifurcations meet for decreasing c and disappear. For c chosen lower than the minimum of the flip curve in figure 7.5 the arc connected to the Γ at (FL1) and (FL2) in Figure 7.3 closes and forms an isolated closed curve. A properly chosen Poincaré section will now show three fixed points: one symmetrical fixed point for Γ and two asymmetrical fixed points, of which one is a saddle, for the two asymmetrical limit cycles. In the fold bifurcations (F2, F3) the two asymmetrical fixed points meet and disappear. At the curve for the fold bifurcation a fixed pointexists with a multiplierat one. In the Neimark-Sacker bifurcation (NS1) an invariant closed curved is formed in the Poincaré map around the stable asymmetrical fixed point. At he Neimark-Sacker curve the two multipliers are complex with real part equal to one. As can be seen in Figure 7.5, the curves for the Neimark-Sacker bifurcation and the fold bifurcation meet in one point. In this codimension two bifurcation point the two asymmetrical fixed points collide and must have two multipliers of value one at

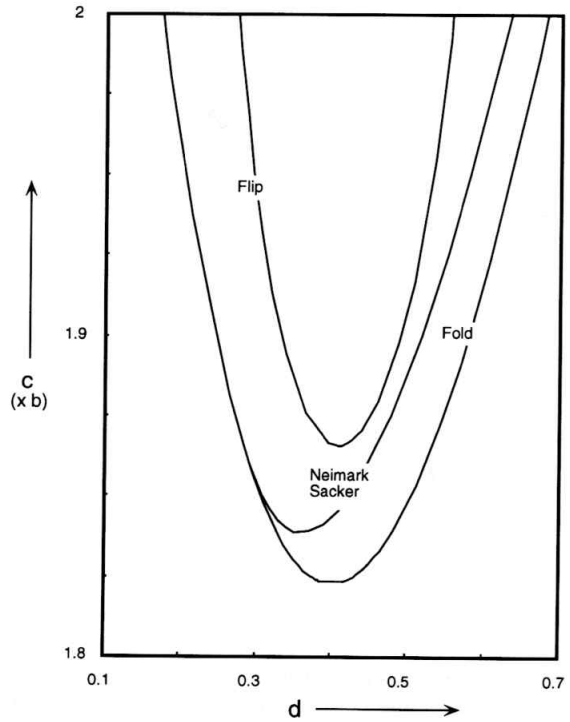

Figure 7.5: A two parameter bifurcation diagram for (7.2) in d and c giving the curves for the flip, Neimark-Sacker and some of the fold bifurcations of figure 7.3. At the point where the Neimark-Sacker curve meets the curve for the fold bifurcation a co dimension two bifurcation point can be found. See the text for explanation. Parameters (except c) as in Figure 7.1.

the point of collision, we will refer to this point as the strong resonance 1:1 point. At the strong resonance 1:1 point also a curve corresponding to a saddle connection or homoclinic bifurcation is attached (not shown in figure, see Arrowsmith & Place (1990) or Kuznetsov (to appear) for a more detailed description of the behaviour around the strong resonance 1:1 point). In the homoclinic bifurcation the invariant closed curve formed in the Neimark-Sacker bifurcation touches the saddle and forms a connection between the stable and unstable manifolds of the saddle. The invariant closed curve disappears in this global bifurcation. The curve for the homoclinic bifurcation lies above the Neimark-Sacker curve in Figure 7.5 (not shown). The homoclinic bifurcation takes place for the Poincaré map and therefore the connection between the stable and unstable manifolds of the saddle fixed points is structurally stable; the stable and unstable manifolds of the saddle intersect not only at the homoclinic bifurcation but in a region situated in parameter space around the curve for the homoclinic bifurcation. In this region the intersections of the stable and unstable manifolds of the saddle

equilibrium create a horseshoe map. The dynamics of the horseshoe map can be chaotic (Wiggins, 1990). The dynamics on the intersecting stable and unstable manifolds is such that the system stays near the saddle for a number of iterations followed by an excursion away from the saddle, then to return again to the neighbourhood of the saddle. The dynamics are chaotic in the sense that the sequence of the numbers of iterations spent in the neighbourhood of the saddle can take any form.

Armed with this knowledge we can now reconstruct the dynamics in the region of Figure 7.3 where no stable attractor is depicted. For a change we will describe the events for decreasing d, i.e. going from left to right in Figure 7.3. For $d > 0.683$ the symmetrical limit cycle Γ is the only stable attractor. When d is decreased below 0.683 two asymmetric limit cycles form in a fold bifurcation (F3), one of these limit cycles is stable, the other is a saddle. The stable limit cycle grows away from the saddle cycle and then loses stability in a Neimark-Sacker bifurcation (NS1). Here an invariant torus is formed around the limit cycle on which stable quasi-periodic solutions live. For decreasing d the torus blows up and grows away from the limit cycle that is enclosed in it. Meanwhile the saddle cycle approaches Γ and disappears in a flip bifurcation (FL2) at $d = 0.558$; the limit cycle Γ then becomes unstable. For d decreased further the torus grows in the direction of an unstable limit cycle and the stable and unstable manifolds of this saddle cycle (this can be either Γ or a saddle cycle that is formed in one of the flip bifurcations) move toward each other and meet. Then the stable and unstable manifolds intersect. Now the dynamics can be either quasi-periodic (for orbits lying on the torus) or chaotic. The chaotic behaviour shows irregular visits to the saddle cycle, mixed with excursions in which the amplitude of the oscillations are decreased (Figure 7.6). Next the torus touches the saddle cycle and disappears. The intersections of the stable and unstable manifolds of the saddle cycle persist and give rise to chaotic dynamics. When Γ is unstable and the invariant torus does not exist, chaotic dynamics will result from almost all initial conditions. For a further decrease of d the intersections of the unstable and stable manifolds of the saddle cycle disappear. Before they disappear totally Γ regains stability in a subcritical flip bifurcation (FL1). Finally, the two asymmetrical unstable limit cycles grow towards each other, collide and disappear in a fold bifurcation (F2).

For small predator migration rates we now have completed the description of the dynamical behaviour. An obvious next question is how this behaviour changes under an increase of c. We remind the reader that the carrying capacity c has a negative feedback on the prey densities und asserts a stabilizing influence on the dynamics. By increasing c the feedback is reduced and in an uncoupled predator-prey system, i.e., system (7.1), the amplitude of the oscillations increases while the minimum density along the limit cycle decreases.

Figure 7.7 gives a two parameter diagram in d and c. For increasing c the curve for the flip bifurcation closes, hence, for large carrying capacities Γ becomes attracting again. The curve for the fold bifurcation widens and encloses a region where asymmetrical attractors exist, indicating that locally asynchronous

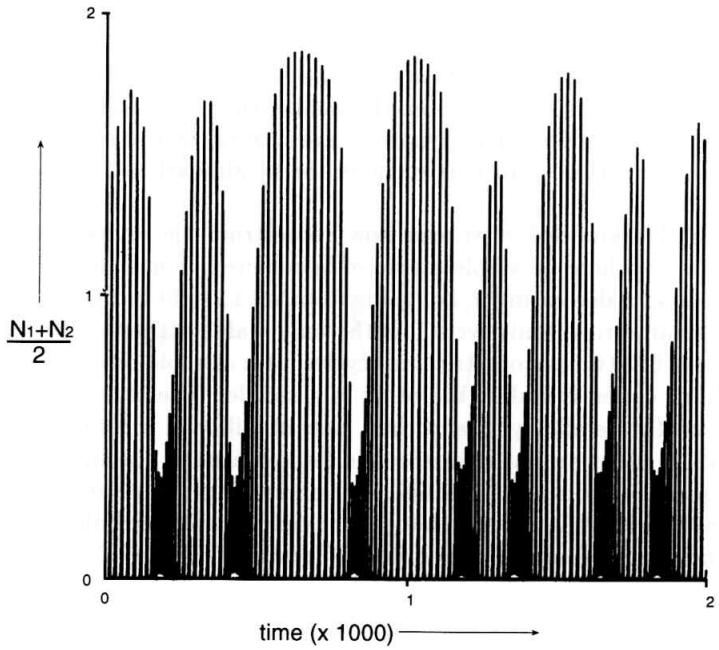

Figure 7.6: The average prey density versus time for a "chaotic" solution of (7.2). Parameter values: $b = 9.96$, $c = 2.5b$, $d = 0.5$, $d_n = 0$, $\mu = 1$, $r = 1$.

dynamics persist with increasing carrying capacities. Since neither the curves for the homoclinic bifurcation nor the formation of ω-limit sets resulting from the intersection of stable and unstable manifolds can be located with the software used, it is unclear in what part of this region asymmetrical attractors can be found. Simulations showed that asymmetrical attractors of the types as dicussed in this subsection, do exist in a large part of this region.

7.3.5 Large predator migration rates

Figure 7.8 shows some of the stable and unstable ω-limit sets in the four dimensional state space for large values of d. Firstly we remark that throughout this range the symmetrical limit cycle Γ is stable (thick horizontal line) but that this limit cycle nowhere is connected to the limit cycle in the face $N_2 = 0$. The equilibrium E_{22a}, denoted by the thin horizontal dashed line, is also unstable for all values of d. From this equilibrium the unstable equilibria E_{22b} and E_{22c} branch off in a pitchfork bifurcation (PE). With increasing d the equilibria move through the positive state towards the faces and leave the positive state space through, respectively, E_{21} and E_{12} in transcritical bifurcations of equilibria (TE). After this bifurcation E_{22b} and E_{22c} are negative and unstable. For increasing d a Hopf bifurcation (H4) can be detected on the unstable equilibrium E_{22b} (and of

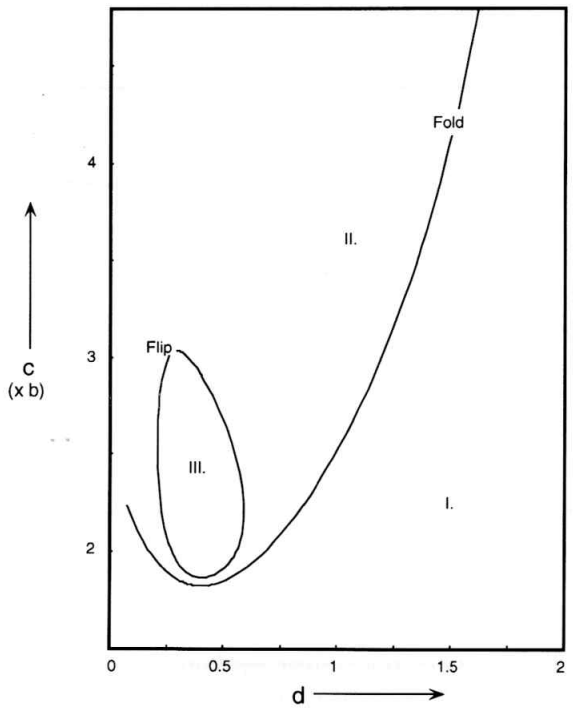

Figure 7.7: As figure 7.5. In regions I. and II. the symmetrical limit cycle Γ is stable, in region III. it is unstable. In regions II. and III. other attractors than Γ can exist.

course on E_{22c} although this is not shown in the figure), where an unstable limit cycle forms on which the prey densities in patch 2 are negative. This limit cycle gains stability for somewhat larger d in a Neimark-Sacker bifurcation (NS2). The now stable limit cycle enters the positive state space through the limit cycle that branched off E_{21} in a transcritical bifurcation of cycles (TC). In this bifurcation the limit cycle transfers its stability to the limit cycle that lies in the face $N_2 = 0$. The stable manifold of the now unstable limit cycle that entered the positive state space forms the separatrix between the attracting domains of the stable limit cycle in the face $N_2 = 0$, the stable limit cycle in the face $N_1 = 0$ and Γ.

When the transcritical bifurcations of equilibria (TE) and the Hopf bifurcation on E_{21} (H4) are continued in a two parameter space, the curves corresponding to these bifurcations cross (Figure 7.9).

At the point of crossing an equilibrium exists with two purely imaginary eigenvalue and an eigenvalue that equals zero. The eigenspace associated with the imaginary eigenvalues lies in the invariant face and the eigenspace associated with the transversal eigenvalue at zero is transversal to the face. Here a Hopf bifurcation takes place in the invariant face simultaneously with a transcritical

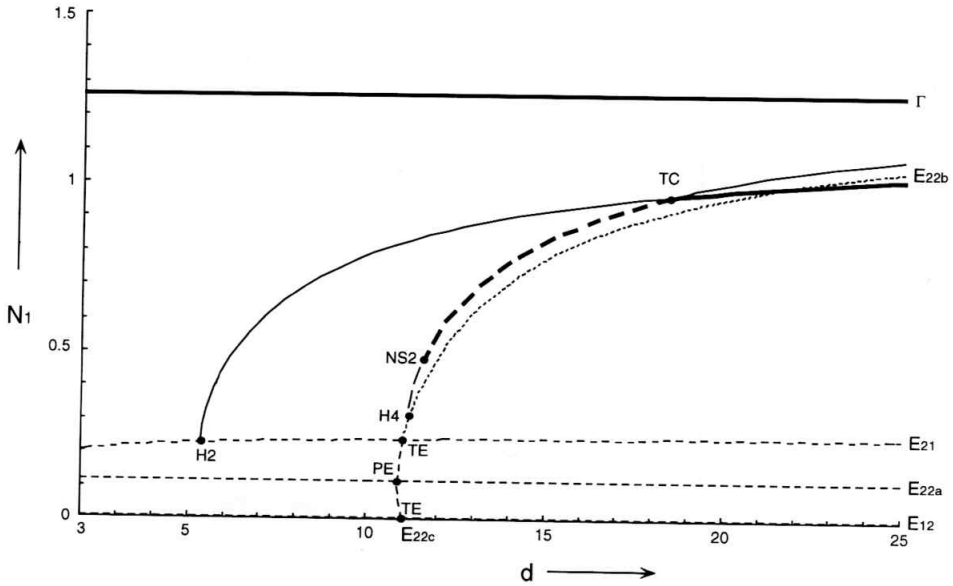

Figure 7.8: As figure 7.3 for large values of d. Dashed lines represent unstable positive equilibria, fine dashed lines unstable non-positive equilibria, thin drawn lines unstable limit cycles, thick drawn lines stable positive limit cycles, thick dashed lines stable non-positive limit cycles. Black dots indicate bifurcations. Labels: H2,H4: Hopf bifurcation, NS2: Neimark-Sacker bifurcation, PE: pitchfork bifurcation of equilibria, TC: transcritical bifurcation of limit cycles, TE: transcritical bifurcation of equilibria. Parameter values as in figure 7.1.

bifurcation in which an equilibrium crosses the invariant face. Curves corresponding to a Hopf bifurcation at the "entering" equilibrium and a transcritical bifurcation of cycles are attached to this codimension two bifurcation point (Klebanoff & Hastings, 1994; McCann & Yodzis, submitted; Jansen, submitted *a*). Figure 7.9 shows these curves. Also the curve for the Neimark-Sacker bifurcation is attached to the point (Klebanoff & Hastings, 1994) (not shown in Figure 7.9). Note that the curve for the pitchfork bifurcation point does not go through the codimension two point since it is associated with equilibrium E_{22a} which cannot move out of $\mathbb{R}^4_+$ through E_{12} or E_{21}.

Figure 7.9 shows that for values of c lower than the value of c corresponding to the codimension two bifurcation point, a stable attractor in the face $N_2 = 0$ can be formed through a different scenario (Van der Laan, in prep.). When a cross section through figure 7.9 is made for fixed c below the codimension two bifurcation point the following sequence of bifurcations takes place for increasing d: first a pitchfork bifurcation of the unstable equilibrium E_{22a} (PE) is encountered in which the unstable equilibria E_{22b} and E_{22c} are formed, as in Figure 7.8. These two equilibria gain stability in a Hopf bifurcation (H4) where unstable

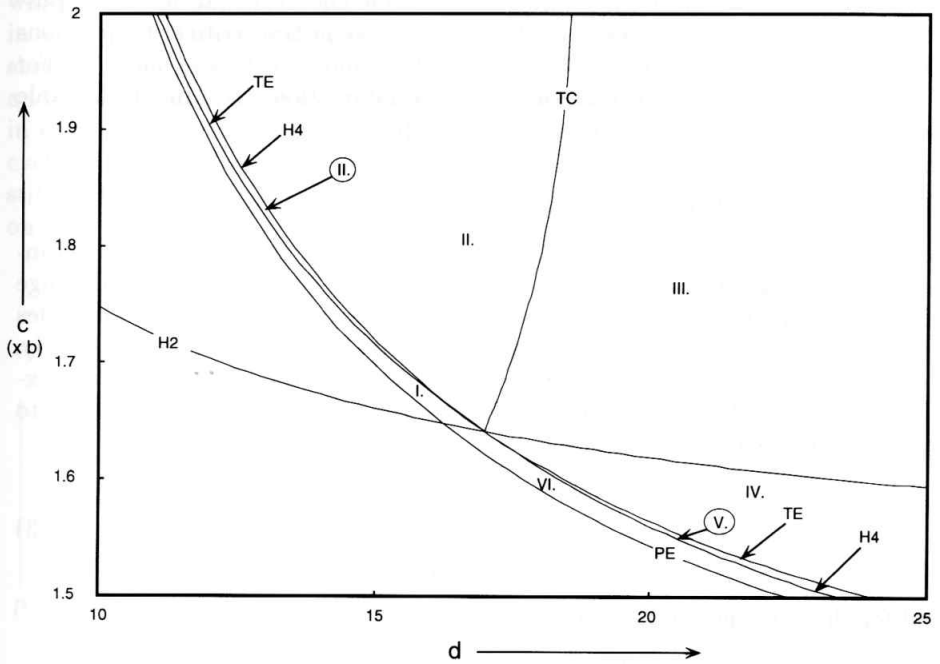

Figure 7.9: A two parameter bifurcation diagram for (7.2) in d and c giving the curves for the Hopf bifurcations on equilibria E_{21} and E_{12} (H2), the Hopf bifurcations on equilibria E_{22b} and E_{22c} (H4), the transritical bifurcations of the equilibria E_{22b} with E_{21} and E_{22c} with E_{12} (TE), the transcritical bifurcation of limit cycles (TC) and the pitchfork bifurcation on equilibrium E_{22a} (PE). At the point where the curves H2, H4, TE and TC cross (note that TE and H4 actually cross) a codimension two bifurcation point exists. Around the codimension two bifurcation six different regions exist with different arrangements of limit cycles and equilibria in the non-negative state space. In region I. two unstable limit cycles and two unstable equilibria lie in the faces $N_i = 0$, the equilibria E_{22b} and E_{22c} are positive and unstable. Region II.: two unstable limit cycles and two unstable equilibria lie in the faces, equilibria E_{22b} and E_{22c} are non-positive and in part of the region surrounded by non-positive limit cycles. Region III.: stable limit cycles and unstable equilibria in the faces, two unstable limit cycles exist in positive state space. Region IV.: two stable equilibria lie in the faces, two unstable limit cycle exist in positive state space. Region V.: two unstable equilibria in the faces, two stable equilibria and two unstable limit cycles lie in positive state space. Region VI. two unstable equilibria in the faces and two unstable equilibria in positive state space. In all regions Γ is stable and equilibrium E_{22a} is unstable. Parameters (except c) as in figure 7.1.

limit cycles branch off. The stable manifolds of these limit cycles form the separatrices between the domains of attraction of E_{22b}, E_{22c} and the attracting symmetrical limit cycle Γ. For larger d the stable equilibria can leave the positive state space through, respectively, E_{12} and E_{21} in transcritical bifurcations (TE). The stability then is transferred from E_{22b} and E_{22c} to E_{12} and E_{21}. For d still larger E_{12} and E_{21} can go through Hopf bifurcations (H2) in which stable limit cycles in the faces $N_i = 0$ come into existence.

7.3.6 Exponential prey growth

Although the diagram in Figure 7.7 illustrates some of the consequences of increased carrying capacity, the figure only gives results for a relatively small range of carrying capacities. For larger values of c continuation for some limit cycles becomes numerically difficult, whereas other limit cycles can be continued easily. Therefore we will further concentrate on the the case where prey growth is exponential, which can be derived from (7.1) and (7.2) by taking the limit of c to infinity. This results in the equations:

$$\begin{aligned} \frac{dN}{dt} &= rN - \frac{NP}{1+N/b} \\ \frac{dP}{dt} &= \frac{NP}{1+N/b} - \mu P \end{aligned} \tag{7.3}$$

and for the corresponding two patch system:

$$\begin{aligned} \frac{dN_i}{dt} &= rN_i - \frac{N_iP_i}{1+N_i/b} + d_n(N_j - N_i) \\ \frac{dP_i}{dt} &= \frac{N_iP_i}{1+N_i/b} - \mu P_i + d(P_j - P_i) \end{aligned} \qquad i,j \in \{1,2\}; \quad i \neq j \tag{7.4}$$

System (7.3) maximally allows for three equilibria with zero, one or two species present. The two species equilibrium is an unstable focus when it exist. Solutions of (7.3) show oscillations over which the predator and prey densities become unbounded and can be brought to arbitrarily large and small values. Simulation runs of system (7.4) show that the diagonal subspace D, which contains all symmetrical solutions, is attracting. For larger d orbits can also converge to one of the faces $\{(N_1, P_1, N_2, P_2) \in \mathbb{R}^4_+ | N_i = 0, i = 1, 2\}$, in which the orbits also show unbounded divergent oscillations. Yet, for suitable chosen initial conditions also bounded fluctuations are possible.

Figure 7.10 gives a partial bifurcation diagram in d for system (7.4). As before we have chosen the prey migration, d_n, zero. The equilibrium E_{22a} is represented by the horizontal dashed line. On this equilibrium a Hopf bifurcation takes place from which a limit cycle is born, on this cycle the local densities in the patches fluctuate with a phase difference of π (see the phase portrait in Fig. 7.10). From in which the densities in one of the patches are close to the two species equilibrium while in the other patch the densities oscillate regularly. This part of the picture is identical to that of Figure 7.3. Then, the limit cycle born from E_{22a} turns back in a fold bifurcation, goes through a pitchfork bifurcation

in which two limit cycles branch off (only one of these limit cycles is shown in figure 7.10) and completes a loop by turning again in another fold bifurcation in which a stable limit cycle is formed. The stable limit cycle then loses stability in a Neimark-Sacker bifurcation where a torus forms around the limit cycle (not shown). The now unstable cycle goes through a number of other bifurcations and forms new loops. In every loop in the bifurcation diagram also a loop forms in the phase portrait (Figure 7.10). We note that the stable asymmetrical limit cycle of figure 7.3 can be continued to the stable limit cycle of figure 7.10. It is still unclear how, along this path, the connection with the Hopf bifurcation (H1) on E_{22a} is formed.

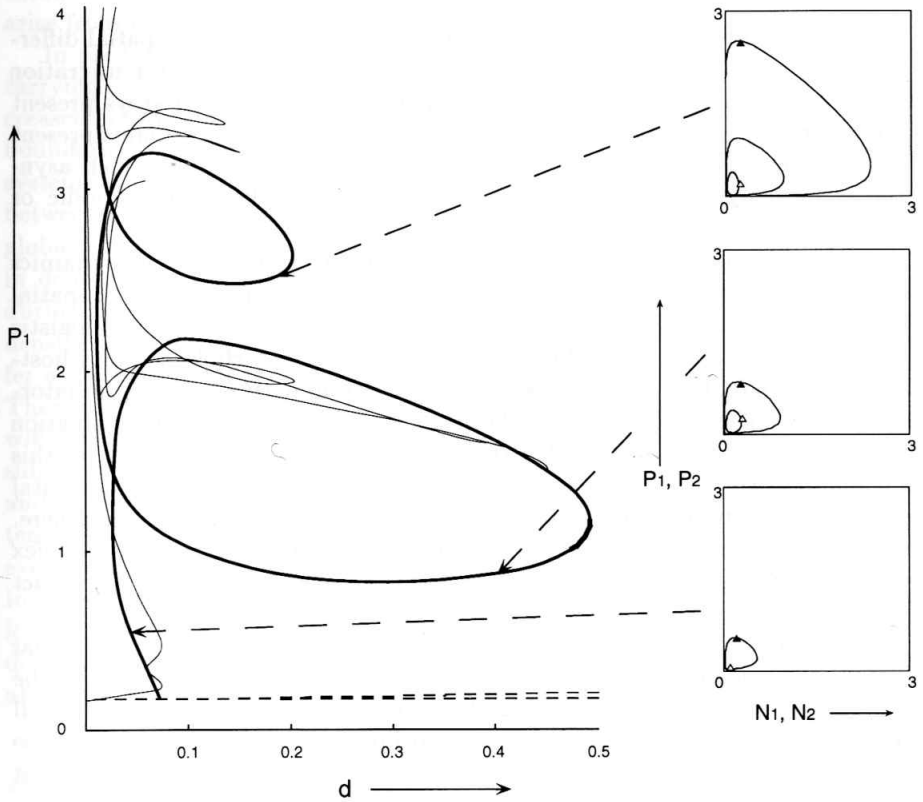

Figure 7.10: A one parameter bifurcation diagram for (7.4). The equilibrium values of P_1 or the maximum of P_1 over the limit cycle is plotted against d. Dashed lines represent unstable equilibria, thin and very thin drawn lines unstable limit cycles and thick drawn lines stable limit cycles. Note that the dashed lines for equilibria E_{21} and E_{22a} lie very close to each other. The limit cycle is formed from a Hopf bifurcation on E_{22a}. The insets are the phase portraits for a number of limit cycles. The solid and open triangles give the position of the densities at the same moment for the different patches.

The pattern of loops that can be observed in Figure 7.10 can result from a homoclinic bifurcation, known as Sil'nikovs phenomenon (Glendinning & Sparrow, 1984). Although the phase portraits confirm that with every loop the limit cycles spend more time in the neighbourhood of E_{12} or E_{21}, it is unclear how such a global bifurcation could take place. Since our aim is merely to demonstrate that in a two patch system bounded asynchronous solutions are possible in total absence of regulation through a limited carrying capacity, a complete analysis of the behaviour of (7.4) lies beyond the scope of this paper.

7.4 Discussion

In a two patch predator-prey model with only predator migration spatial differences can persist. This can happen in two ways: for larger predator migration rates the prey can disappear asymptotically in one patch while it stays present in the other patch. For small predator migration rates the prey remains present in both patches while the local densities fluctuate asynchronously. Such asynchronous local dynamics can come in the form of periodic, quasi-periodic or chaotic behaviour.

Vandermeer (1993) found behaviour qualitatively similar to the dynamics found here in a loosely coupled predator-prey system. The persistence of spatial differences has also been demonstrated two patch sytems with coupled logistic maps (Gyllenberg *et al.*, 1993; Hastings, 1993) and with a Nicholson-Bailey host-parasoid system (Adler, 1993). This seems a general property of spatial predator-prey systems. The paper by Adler shows that also for positive prey migration rates, spatial differences persist. For the coupled logistics it was shown that this behaviour persists under differences in the within patch dynamics. Incidental observations clearly indicated that the same holds for the systems studied here. Since the two patch predator-prey model turned out to behave far more complex than we initially expected and we will not digress in speculations about the exact bifurcation structures.

Our results not only have a meaning for two patch systems. For similar predator-prey systems that "live" on large grids, spatial patterns arise from the interplay between migration and local dynamics (De Roos *et al.* 1991; Hassell *et al.*, 1991; Comins *et al.*, 1992). The asynchrony of local dynamics has also been demonstrated in an experimental predator-prey system (Van de Klashorst *et al.*, 1992; Lingeman & Van de Klashorst, 1992). Interestingly, the densities in the different compartments of the experimental system fluctuated in phase for about a year, then to proceed out of phase for another year. This resembles the dynamics of the model system in this paper where the symmetrical limit cycle, on which the densities fluctuate in phase, can be stable or weakly unstable while attractors with asynchronous local dynamics exist.

The fact that spatial differences can be maintained in homogeneous predator-prey systems confirms one of the essential presumptions of metapopulation theory. The mechanism behind the asynchrony of the local dynamics, possibly is

somewhat different from what it is often believed to be. It is often argued that asynchronous local dynamics will arise from environmental differences between patches (Taylor, 1990). Our results show that environmental differences between patches are not a necessary requirement for asynchronous attractors: in the system studied in this paper both the symmetrical limit cycle and an asymmetrical limit cycle over which the local densities fluctuate asynchronously, can be stable. In a system with small differences between the parameters describing the local dynamics, say in the carrying capacities, the same solution the local dynamics proceed synchronously despite the differences in carrying capacities, while in the other stable solution the local dynamics are asynchronous. Hence, the asynchronous fluctuations need not result from environmental differenced but can arise from the interplay of migration and local dynamics.

In predator-prey systems in a single compartment an increase in the prey's carrying capacity will lead to fluctuations in predator and prey densities with increased amplitudes, bringing the predator and prey populations ever closer to the boundaries of extinction (Rosenzweig, 1971 and 1972). In spatial predator-prey systems the differences in densities can be less extreme through lasting differences between the local densities, preventing the populations to reach densities where global extinction is likely to occur. The mechanism that maintains differences in densities lies in the near to exponential prey growth that can be observed during large fluctuations. During exponential prey growth the difference in prey densities will also grow exponential. Thus, paradoxically, large fluctuations offer a mechanism for the reduction of the fluctuations in an ensemble of patches. Therefore, an increase of the carrying capacity in a spatial predator-prey system will first give rise to an increase in the amplitude of the fluctuations but for a sufficiently large carrying capacity the local dynamics can become asynchronous and the increase in amplitudes stops. A single compartment, predator-prey system with exponential prey growth and a Holling type II functional response will eventually drive itself to extinction due to the absence of density dependence. In a predator-prey system with more compartments the interplay of spatial and local interactions can regulate the populations in total absence of density dependence at the level of the individual. Seen this way there is nothing paradoxical about the enrichment of predator-prey systems.

Acknowledgements

I am indebted to Pavel Brunovski for many inspiring discussions and to Odo Diekmann for commenting the manuscript. I gratefully acknowledge the financial support of the Austrian Forschungs Förderungs Fonds, nr. 8043.

7.5 Appendix Computation of the equilibria

The equilibria of (7.2) with $d_n = 0$ are the roots of the following system of equations:

$$rN_i(1 - \frac{N_i}{c}) - \frac{N_i P_i}{1 + N_i/b} = 0 \tag{7.5}$$

$$\frac{N_i P_i}{1 + N_i/b} - \mu P_i + d(P_j - P_i) = 0 \tag{7.6}$$

Clearly, when $P_1 = P_2$ the roots are:

$$N_i = 0 \vee P_i = 0, \qquad N_i = c \vee P_i = 0, \qquad \text{or} \quad N_i = N^* \vee P_i = \frac{r}{\mu} N^*(1 - \frac{N^*}{c})$$

where

$$N^* = (\frac{1}{\mu} - \frac{1}{b})^{-1}.$$

These roots correspond to the equilibria E_{00}, E_{11} and E_{22a}, respectively.

When $N_j = 0$ we have the relation: $P_j = \frac{d}{d+\mu} P_i$. After substituting this relation in (7.6) we find the root:

$$N_i = \tilde{N}, P_i = \frac{r(d+\mu)}{\mu^2 + 2d\mu} \tilde{N}(1 - \frac{\tilde{N}}{c}), N_j = 0, P_j = \frac{dr}{\mu^2 + 2d\mu} \tilde{N}(1 - \frac{\tilde{N}}{c})$$

where

$$\tilde{N} = (\frac{d+\mu}{\mu^2 + 2d\mu} - \frac{1}{b})^{-1},$$

corresponding to the equilibria E_{12} and E_{21}.

When both $N_i > 0$ and $N_j > 0$ matters are somewhat less straightforward. Elimination of P_i and P_j gives:

$$(1 - \frac{N_i}{c})((\mu + d)(1 + \frac{N_i}{b}) - N_i) = d(1 - \frac{N_j}{c})(1 + \frac{N_j}{b})$$

so that the problem reduces to the finding of the roots of:

$$(c - N_1)((\mu + d)(1 + \frac{N_1}{b}) - N_1) = (c - N_2)(d + \frac{d}{b} N_2) \tag{7.7}$$

$$(c - N_1)(d + \frac{d}{b} N_1) = (c - N_2)((\mu + d)(1 + \frac{N_2}{b}) - N_2). \tag{7.8}$$

By subtracting the two equations from each other we find:

$$(N_i - 1/2(c + N^*))^2 + (N_j - 1/2(c + N^*))^2 = 1/2(c - N^*)^2 \tag{7.9}$$

which expresses that the equilibrium values of N_1 and N_2 lie on a circle in the N_1, N_2 plane. Multiplication of (7.7) by $(\mu + d)(1 + \frac{N_2}{b}) - N_2$ and (7.8) by $-(d + \frac{d}{b}N_2)$ gives after addition:

$$\left(((\mu + d)(1 + \frac{N_1}{b}) - N_1)((\mu + d)(1 + \frac{N_2}{b}) - N_2) - d^2(1 + \frac{N_1}{b})(1 + \frac{N_2}{b})\right) \times (c - N_1) = 0$$

from which N_2 can be solved, under the condition that $N_1 \neq c$:

$$N_2 = \frac{(N^* + 2\gamma)N^* - \gamma N_1}{\gamma + N_1} \tag{7.10}$$

where

$$\gamma = \frac{b(2d\mu + \mu^2 - bd - b\mu))}{(b - \mu)(b - \mu - 2d)}$$

By plugging in (7.10) in (7.9) and multiplying both sides by $(\gamma + N_1)^2$ we find:

$$(N_1 - N^*)^2 \left(N_1^2 + 2\left(\gamma + \frac{1}{2}(N^* - c)\right)N_1 + (N^* + \gamma)^2 + \gamma(\gamma + N^* - c)\right) = 0$$

Clearly, the polynomial has a double root at N^* and the other two at:

$$\hat{N}_a = \frac{1}{2}(c - N^*) - \gamma + \frac{1}{2}\sqrt{(c - 3N^* - 2\gamma)(N^* + c + 2\gamma)}$$

$$\hat{N}_b = \frac{1}{2}(c - N^*) - \gamma - \frac{1}{2}\sqrt{(c - 3N^* - 2\gamma)(N^* + c + 2\gamma)}$$

Hence, the equilibria E_{22b} and E_{22c} are given by:

$$E_{22b} = (\hat{N}_a, r(1 - \frac{\hat{N}_a}{c})(1 + \frac{\hat{N}_a}{b}), \hat{N}_b, r(1 - \frac{\hat{N}_b}{c})(1 + \frac{\hat{N}_b}{b}))$$

$$E_{22c} = (\hat{N}_b, r(1 - \frac{\hat{N}_b}{c})(1 + \frac{\hat{N}_b}{b}), \hat{N}_a, r(1 - \frac{\hat{N}_a}{c})(1 + \frac{\hat{N}_a}{b}))$$